

Short communication

Enhancing photovoltaic applications through precipitating agents in ITO/CIS/CeO₂/Al heterojunction solar cell

P. Gayathri^a, T. Akila^a, G. Alan Sibu^a, Manickam Selvaraj^{b,c}, Mohammed A. Assiri^{b,c}, Priyadarshini Matheswaran^d, V. Balasubramani^{a,*}

^a Department of Physics, Saveetha School of Engineering, Saveetha Institute of Medical and Technical Sciences, Saveetha University, Chennai 602 105, Tamil Nadu, India

^b Department of Chemistry, Faculty of Science, King Khalid University, Abha 61413, Saudi Arabia

^c Research Centre for Advanced Materials Science (RCAMS), King Khalid University, PO Box 9004, Abha 61413, Saudi Arabia

^d Department of Physics, Vel Tech Rangarajan Dr. Sagunthala R&D Institute of Science and Technology, Avadi, Chennai 600 062, India

ARTICLE INFO

Keywords:

CeO₂-NPs
Chemical precipitating agents
JNSP
Heterojunction
Solar cell
Optoelectronic applications

ABSTRACT

In this groundbreaking study, we successfully synthesized both cerium oxide and copper indium sulphate nanoparticles via co-precipitation method and the same is spray coated on ITO substrate by Jet Nebulizer Spray Pyrolysis (JNSP) technique. A comprehensive characterization of the structural, morphological and Photo-diode properties was conducted using a range of advanced techniques. X-ray diffraction revealed a superior monocrystalline cubic fluorite structure with a preferred orientation along the (111) plane, indicating exceptional crystal quality. Scanning electron microscopy and transmission electron microscopy images showed the formation of disk-shaped particles with sharp rounded edges, averaging ~ 5 nm in size. Fourier transform infrared spectroscopy identified the phonon band envelope of the metal oxide (CeO₂) network at 848 cm⁻¹ while photoluminescence spectroscopy revealed blue and blue-green emission in the visible spectrum. Thermogravimetric-differential thermal analysis exhibited a total weight loss of 19.52 % with four distinct exothermic and endothermic peaks. X-ray photoelectron spectroscopy confirmed the presence of Ce and O elements, with a minor amount of carbon absorbed from the atmosphere and revealed the dominant occurrence of Ce⁴⁺ and minority occurrence of Ce³⁺. The maximum power conversion efficiency of 0.23 % was achieved for samples prepared using NH₃ precipitant making them highly suitable for photovoltaic applications. This work paves the way for future research in optimizing cerium oxide nanoparticles for high-performance photovoltaic devices potentially leading to breakthroughs in renewable energy harvesting.

1. Introduction

The human society facing two essential challenges like energy paucity and environmental pollution for the production of efficient devices. To resolve these two challenges, many global researchers have been focused their research to develop highly efficient and low-cost photovoltaic devices for the betterment of future energy crisis [1]. Among various types of solar cells thin film are solar cells are inexpensive and highly efficient, they have attracted a lot of attention because of its high stability, environment friendly, long duration and mass production [2]. US researchers from the University of Delaware first introduced thin-film solar cells (TFSCs) in the 1970s. Owing to the innovative technological advancements TFSCs have attained

remarkable power conversion efficiency so far as 28 % using Copper Indium Gallium Sulfide (CIGS) photoanodes [3]. TFSCs are mostly produced from Chalcogenides, Chalcopyrite's, Perovskites and amorphous silicon. Among these Chalcopyrite-type TFSCs have received considerable interest due to their high absorption coefficient, high environmental stability, and compatibility with manufacturing techniques [4]. In recent years researchers focused their attention to integrate rare earth transition metal oxides (TMO) with chalcopyrite thin films, to fabricate TFSCs with exceptional stability against photo absorption and enhanced electron mobility [5,6,7]. The growing need for cost-effective solar cells that can be scaled up to high power levels worldwide has made (TMO) semiconductors a promising material for these kinds of applications [8,9].

* Corresponding author at: Department of Physics, Saveetha School of Engineering, Saveetha Institute of Medical and Technical Sciences, Saveetha University, Chennai 602 105, Tamil Nadu, India.

E-mail address: balasubramaniv3@gmail.com (V. Balasubramani).

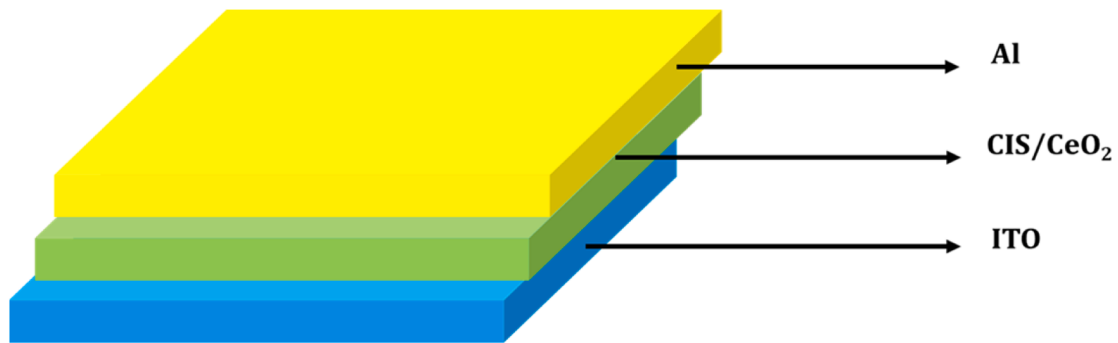
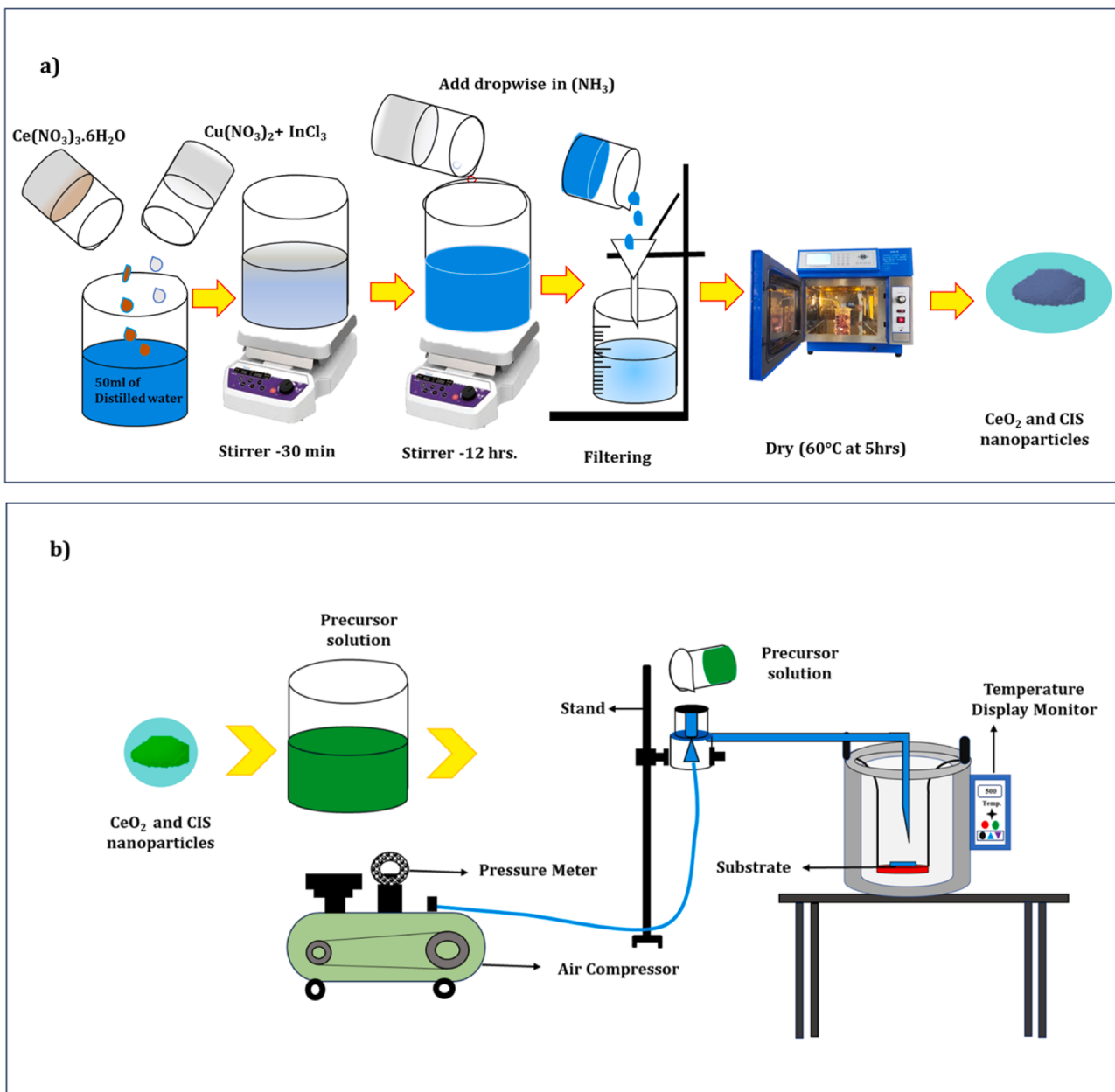


Fig. 1. a) Preparation of CeO₂ nanoparticles b) CeO₂ and CIS are sprayed by JNSP c) CeO₂ and CIS nanoparticles coated on the ITO substrate.

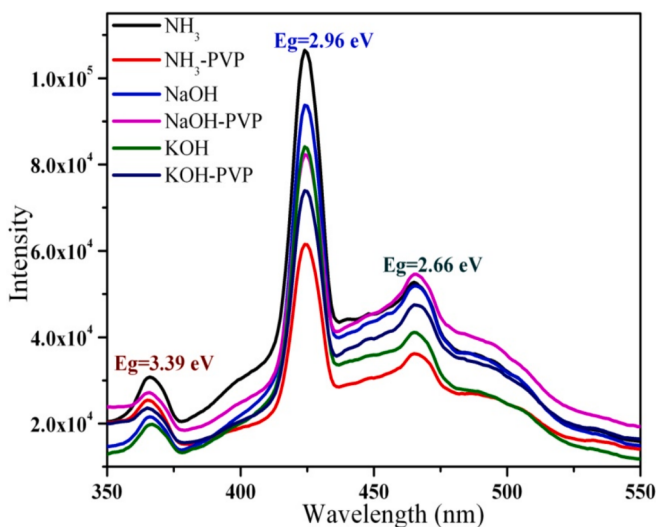


Fig. 2. Room temperature PL spectra of CeO_2 nanoparticles prepared with different precipitants.

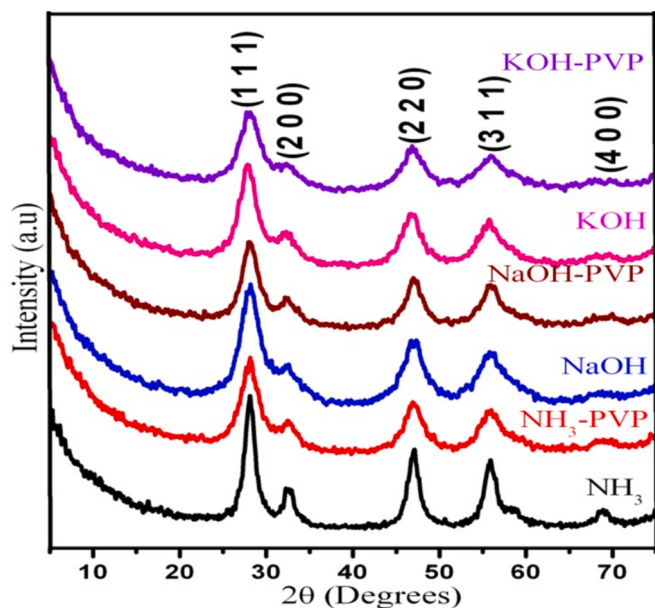


Fig. 4. XRD Patterns of CeO_2 nanoparticles.

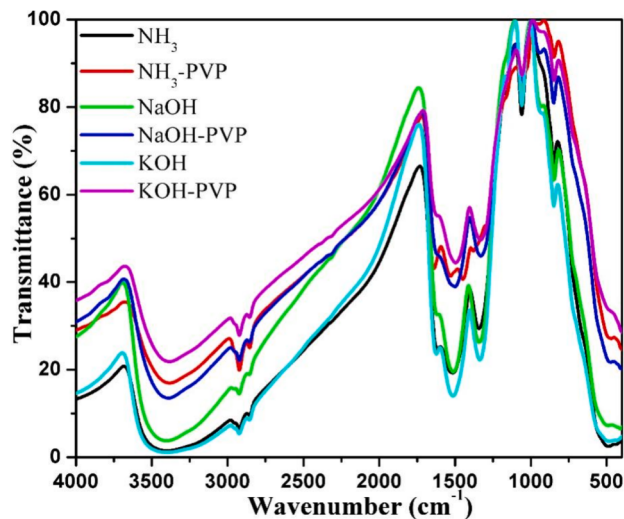


Fig. 3. FTIR spectra of CeO_2 nanoparticles.

The bulk of TMOs have simple manufacturing process, non-toxic raw ingredients and are chemically stable, allowing for material deposition in an atmospheric condition. Particularly, the pairing of large band gap semiconductors with rare earth elements have drawn considerable interest and been recognized for its contributions to catalysis technology [10,11], sensors [12,13], sunscreen materials [14], electrochemical devices [15–17], optoelectronics devices [18,19] and polishing materials [20]. These materials can function as photon converter structures in the solar energy sector with features like down-shifting (DS), Down Conversion (DC) or Up Conversion (UC) it could improve the efficiency of solar cells [21,22]. Rare earth nanoparticle oxides preparation and characterization have drawn a lot of interest because of their remarkably tiny size, high surface area and enhanced characteristics, which makes them act as durable electron acceptors during solar cell preparation [23,24]. Among the most significant rare earth oxides, CeO_2 has a wide range of applications and is desirable material for many technologies. When compared to their bulk counterparts, cerium nanoparticles with large surface area and high thermal stability exhibit unexpected predictable features [25,26]. Among diverse preparation methods, the homogeneous precipitation method [27–30] has induced the curiosity of investigators due to the inherent advantages of being a simple, low cost

and extremely reliable method for creating nanoparticles without adding impurities. The photovoltaic characteristics of cerium oxide nanoparticles are reported by A. Turkovic *et.al.*, M. Lira-Cantu *et.al.*, Y.M Kang *et.al.*, [31–33].

In the present work, we investigate the creation of nanoparticles such as cerium oxide and copper indium sulfate. These nanoparticles are synthesized through a method called Co-precipitation and then deposited onto an ITO substrate using the (JNSP) technique attempted for the first time. This research has potential applications in the development of photovoltaic applications.

2. Experimental part

CeO_2 nanoparticles were synthesized using cerium nitrate $[\text{Ce}(\text{NO}_3)_3]$, poly vinylene pyrrolidine (PVP), aqueous ammonia (NH_3), potassium hydroxide (KOH) and sodium hydroxide (NaOH). In this process, Cerium nitrate hexahydrate (0.1 M) having the chemical formula $\text{Ce}(\text{NO}_3)_3 \cdot 6\text{H}_2\text{O}$ is dissolved in (50 ml) deionized water, stirred vigorously for 30 min and then added to (25 ml) of aqueous ammonia solution, which is added in drops over a 20-minute period. The mixture is then stirred for 12 hrs at room temperature. The solution turns light brown colored gel, when the few drops of ammonia added to the above solution. The color of the initial solution is change from light orange to light black within one hour. After 3 h, the color of the solution is changed to brown, after 7 h, the light brown colored slurry is observed, the pale-yellow colored slurry is obtained at the end of the reaction. It is believed that chemical alterations and the phenomena of color change are related. Ce^{3+} ion transformed to Ce^{4+} by O_2 under the environment of air as the color of reaction solution changed from lite orange into pale yellow [34]. The resulting slurry is filtered and repeatedly rinsed in ethanol and de-ionized water. The oven is used to dry the cleaned powder for 5 h at 60°C . For different forming precipitates agents, such as the elements potassium hydroxide and sodium hydroxide, the same experimental strategy is applied. The schematic and synthetic process of our work is described in the Fig. 1.

To describe the characteristics of the collected samples, various complementary methods are used at room temperature, vibrational measurements are made using the conventional KBr disc technique. A spectrometer, Bruker IFS Table 88 is used to capture IR spectra in the range $4000\text{--}400\text{ cm}^{-1}$. The Bruker (AXS D8 Advance X-ray diffractometer) with XPERT-PRO used to evaluate the purity, crystallinity of the as-

Table 1
Structural parameters of cerium oxide nanoparticles.

Sample name	2 Theta (degree)	FWHM	(hkl)	Crystallite Size (nm)	Texture Coefficient	Lattice Constant (nm)
NH ₃	28.0853	0.6298	111	13.5	0.92955	5.5031
	32.4167	0.9446	200	19.1	0.79043	5.5238
	47.1094	0.6298	220	14.3	1.05290	5.4564
	55.9404	0.7872	311	11.9	1.07562	5.4517
	68.9390	1.1520	400	18.7	1.15148	5.4441
NH ₃ -PVP	28.2762	1.4377	111	5.9	0.87531	5.4667
	32.5346	0.3100	200	7.8	1.03520	5.5043
	46.9649	1.3692	220	6.6	0.90037	5.4722
	56.0990	0.4284	311	7.9	0.78278	5.5225
	69.2310	0.3072	400	6.8	1.40597	5.4584
NaOH	28.28	0.7564	111	11.3	1.03916	5.4660
	32.9256	0.1628	200	13.8	0.96469	5.4711
	47.0669	0.3846	220	12.1	1.06114	5.4611
	56.0578	0.1123	311	13.6	0.93500	5.4411
	27.9975	0.4840	111	7.6	1.00968	5.5200
NaOH-PVP	32.5800	0.4425	200	9.5	0.87203	5.4969
	46.9737	0.3897	220	9.2	1.11725	5.4713
	55.7900	0.3000	311	8.9	1.00103	5.4570
	28.2340	0.0909	111	13.5	1.09588	5.4747
	32.3000	0.5307	200	12.2	0.80474	5.5432
KOH	46.9609	0.2782	220	12.5	1.04783	5.4727
	55.9522	0.3634	311	15.8	1.05153	5.4506
	27.7700	0.5610	111	10.2	1.00779	5.5643
	32.4500	0.6154	200	11.0	1.11025	5.5183
	46.9957	0.7181	220	10.5	0.94422	5.4689
	56.0679	0.1988	311	10.8	0.93772	5.4402

prepared and annealed samples through X ray diffraction. TG/DTA measurement are carried out in a nitrogen atmosphere using TG/DTA 6200 and SII nanotechnology. In a ceramic sample boat heated to 900°C at 20°C/min and in a stream of nitrogen gas at the rate of 40 ml/min, sample weighting 20.0 ± 0.1 mg are placed. Using the (JEOL Model JSM – 6390LV) instrument for high resolution surface imaging and Philips (CM20 Super Twin microscope) respectively, TEM and SEM are used to analyse the samples surface morphology. The preparation of specimens for TEM involves dispersing a powder sample using ultrasonic dispersion in ethanol and placing a solution drop on copper microscope grid. For the analysis of material's chemical and electronic structure, XPS is a straightforward and non-destructive method. The Keithley electrometer 6517B is used to analyse I-V characteristics in the present work.

3. Result and discussion

3.1. Optical analysis

The technique of PL spectroscopy holds great significance in the identification of structural defects and impurities present in materials. Fig. 2 displays the room temperature photoluminescence spectra of CeO₂ nanoaggregates made with various precipitants. These spectra were obtained using a 325 nm xenon laser as the excitation source. It exhibits two low intensity peaks in the Ultra Violet region at 366 nm (3.39 eV), a strong blue emission band in the visible spectrum at 425 nm (2.96 eV) then faint and broad blue-green emission band in the visible spectrum at 466 nm (2.66 eV). The direct recombination of electrons with holes between the Ce 4f conduction band and the O_{2p} valence band is responsible for the weak emission peak seen at 366 nm in the Ultra Violet region [35]. The intense and distinct blue emission peak centered at 425 nm attributed to the creation of point defects, such as oxygen vacancies, on surface of Ce lattice sites. These defect energy levels are situated between the conduction band of Ce 4f and the valence band of O_{2p}, which depends on the temperature and packing density. Furthermore, low-density oxygen vacancy in the sample is proposed to be the cause of the faint and broad blue-green emission peak at 466 nm [36]. The peak intensities of all the samples are compromised by the addition of PVP. Due to the chemical inertness of the precipitants, incorporation of PVP significantly decreases the peak intensities of the samples made

from NH₃ precipitant, while considerably reducing those from NaOH precipitant but hardly reducing those made from KOH precipitant. Interestingly, samples prepared with ammonia precipitant exhibit the highest photoluminescence (PL) intensity peaks, while those treated with PVP dispersant show the lowest, highlighting the dominant emission properties of samples prepared from ammonia precipitant in comparison to other precipitants.

3.2. FT-IR analysis

CeO₂ NPs synthesized with various precipitating agents (NH₃, NaOH and KOH) are displayed in the Fig. 3. The results demonstrate that the greatest intense bands are discovered at (3417, 1506 and below 700) cm⁻¹, whereas weaker intense bands were detected at (2926–2851, 1744, 1629, 1415, 1341, 1170–1000 and 848) cm⁻¹ respectively. The following bands can be attributed to the observed bands: The strong bands at (3417 and 1629) cm⁻¹ are attributed to O—H stretching and H—O—H bending vibration modes indicating that it contains water molecules. This is because the prepared sample absorbs atmospheric moisture and hydroxyl groups are often present and can be removed by heat treatment. [37]. The organic fraction γ (C—H) species and γ (CH₂) were identified by weak methods using bands between 2926 and 2851 cm⁻¹, respectively. The sharp band at 1415 cm⁻¹ is due to the —CH₃ deformation and —CH₂ scissoring vibration of PVP. The presence of C=O, COO— and C—O stretching modes on the ceria surface is most likely related to the additional bands observed at (1744, 1341 and 1170–1000) cm⁻¹ respectively. It has been suggested that carbon dioxide is a sign of the high alkalinity of O₂ ions on the surface of the product and is an approximate adsorbent of the cerium surface at room temperature. This indicates that the carbonate surface type plays an important role in controlling the surface area and porosity of the product. There is no clear evidence for the presence of cerium nitrate (1380 cm⁻¹) in the precursor due to overlapping peaks [38]. It also unveiled the presence of tenacious and broad band obtained at 848 and 400 cm⁻¹ due to the vibrational bands of metal oxide (CeO₂) [39]. Influence of precipitants on the growth of certain vibrational bands and the impact of PVP assimilation on the transmittance of samples. According to Fig. 3, precipitants notably affect the growth of O—H, H—O—H and carbonate bands (C=O and COO—), with marginal effects on C—O stretching vibrations. The

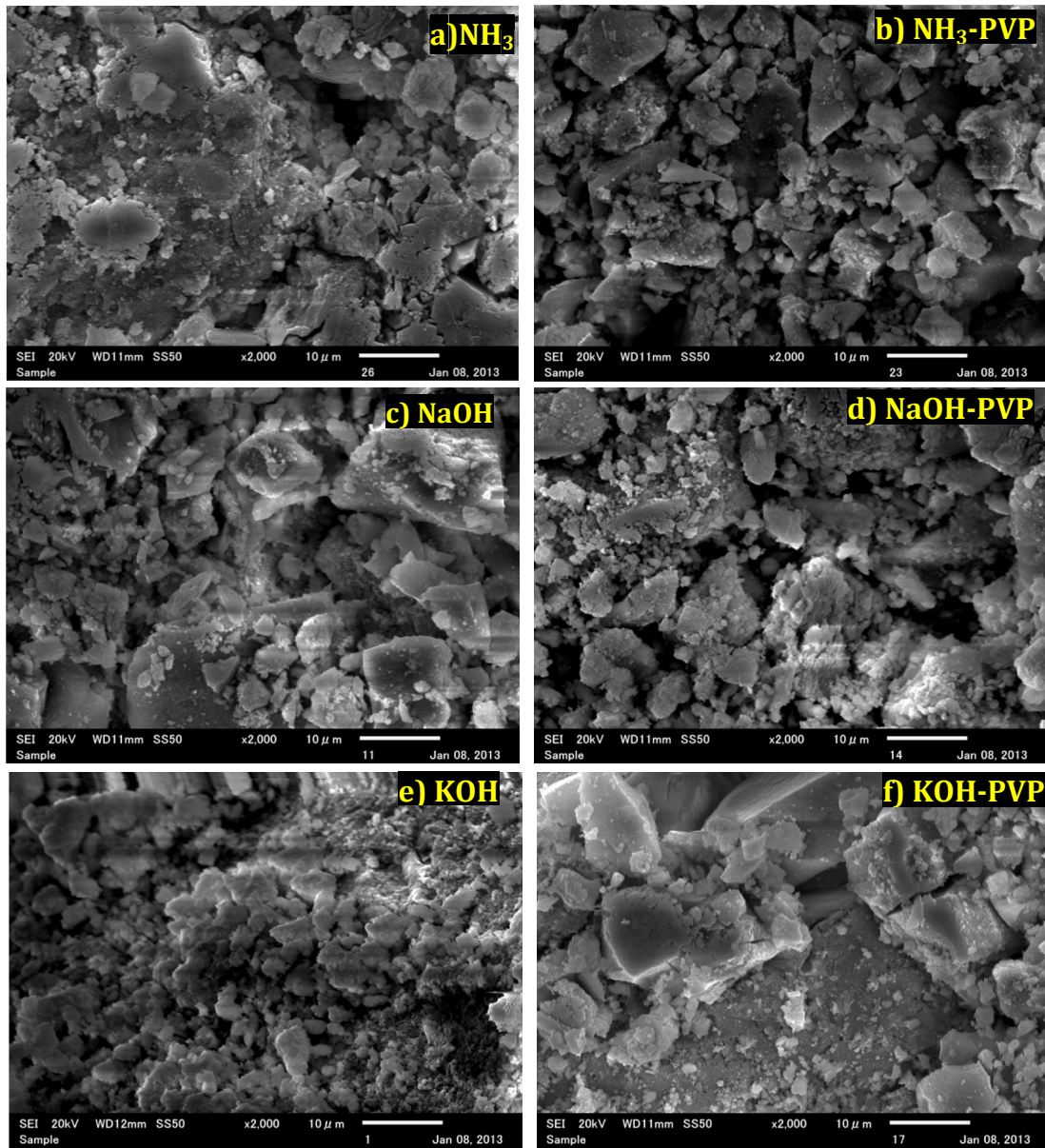


Fig. 5. a-f SEM images of CeO_2 nanoparticles prepared with different precipitants.

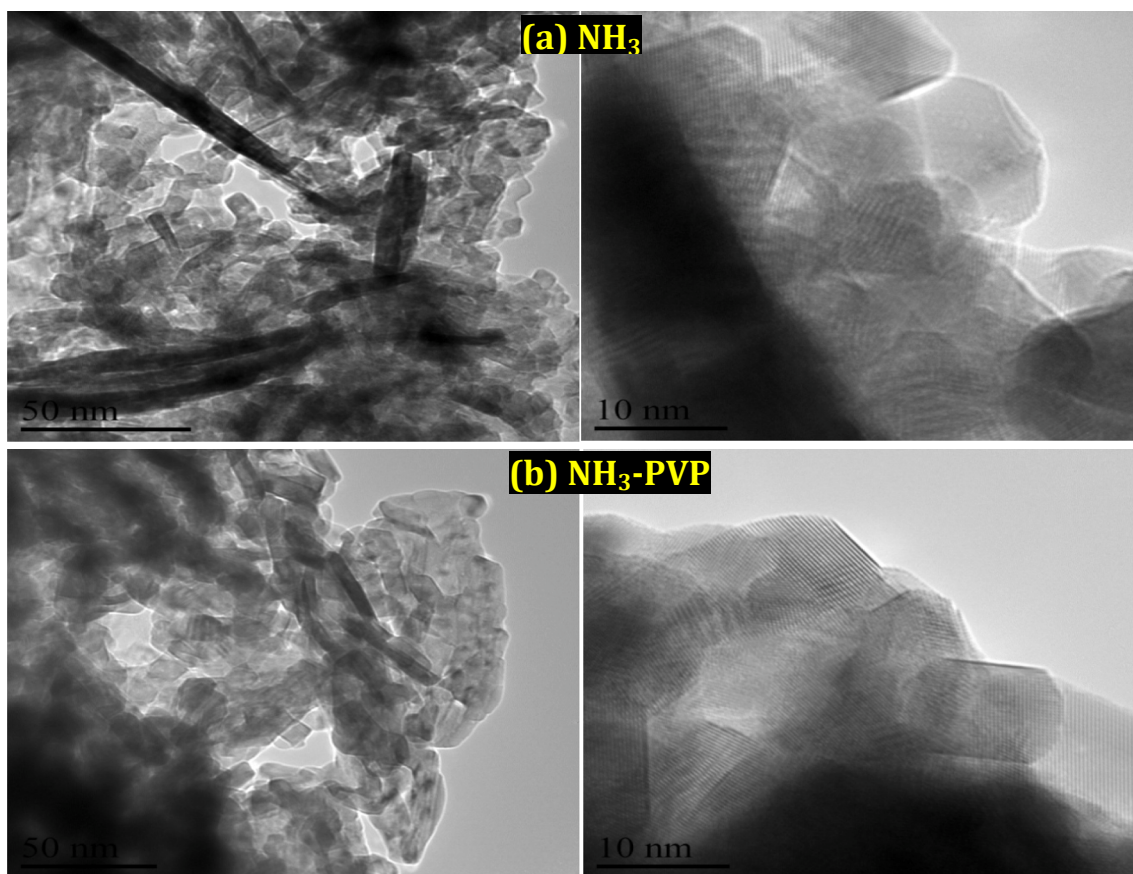


Fig. 6. a, b TEM images of CeO_2 nanoparticles.

incorporation of PVP significantly enhances the transmittance of the samples made from KOH precipitant, marginally affects those from NH_3 precipitant, and substantially increases samples from NaOH precipitant. Despite contradictory results from PL and FT-IR spectra, it is concluded that samples prepared from NH_3 precipitant exhibit superior emission properties and outstanding functional group presence compared to others.

3.3. Structural analysis

Cerium oxide nanoparticles produced using various precipitating agents showing their X-ray diffraction pattern. Fig. 4. illustrates the pattern, revealing diffraction peaks corresponding to the standard JCPDS (34–0394) and aligning with the (1 1 1) (2 0 0) (2 2 0) (3 1 1) and (4 0 0) planes of a face-centered cubic (FCC) structure. The XRD pattern showed a single-phase polycrystalline structure as there was no evidence of a crystalline Ce_2O_3 phase. Notably, all samples, when prepared with various precipitants along with a dispersant, exhibit a preferred orientation along the (1 1 1) direction. This suggests that the precipitants do not alter the orientation of crystallites, and there is no hindrance to the growth of crystallites at specific orientations in the Ce lattice sites. Broad diffraction lines observed in the (XRD) pattern, indicating a reduced crystallite size based on Scherer's equation. A predicted crystallite size falls within the range of 5.9 to 19.1 nm. The influence of a dispersant on the prepared nanoparticles is noted to have a reducing effect on crystallite size, a favourable outcome for improved photovoltaic applications. Table 1 is referenced for the listing and calculation of various structural parameters. According to PL results, lattice strain in the Ce^{3+} sites is identified as the cause of modification in the lattice parameter, leading to the generation of point defects such as oxygen vacancies [40]. It emphasizes that the structural properties of samples synthesized with

NH_3 precipitant are significantly distorted by the dispersant PVP, while those from NaOH and KOH precipitants experience minimal distortion. This observation aligns with the same results obtained from PL analysis.

3.4. Morphological analysis

SEM micrographs for the CeO_2 NPs synthesized from different precipitants as shown in the Fig. 5.a-f. The samples made from NH_3 precipitant (Fig. 5a) exhibit loosely agglomerated spheroidal shaped particles consolidated with dense microstructure of some voids. NaOH precipitant results in aggregates of randomly oriented particles as shown in the Fig. 5c, while KOH precipitant forms a granular structure comprising of uneven and irregular shaped particles in the Fig. 5e. The addition of the dispersant PVP transforms the particle morphology from agglomerated to spheroidal obtained from NH_3 and KOH precipitants.

TEM images of NH_3 -precipitated samples (Fig. 6a) reveal severe agglomeration of spherical particles forming disk-shaped particles with sharp, rounded edges and an average size of 5 nm [41]. Dispersant PVP alters the morphology of the particles, transforming them from disk-shaped to an agglomeration of slap-like particles with curved edges and an average size of 8 nm, as depicted in Fig. 6b. It suggests that these morphological changes contribute to enhancing the photovoltaic properties of the prepared samples.

3.5. Thermal analysis

Fig. 7 (a) and (b) shows the TG-DTA traces of disk and slap-shaped ceria nanoparticles. The samples acquired a 19.52 % overall weight loss with four separates temperature peaks. The release of the water molecules from the precursor was thought to be the cause of the first endothermic peak, which was centered at 120°C. The elimination of

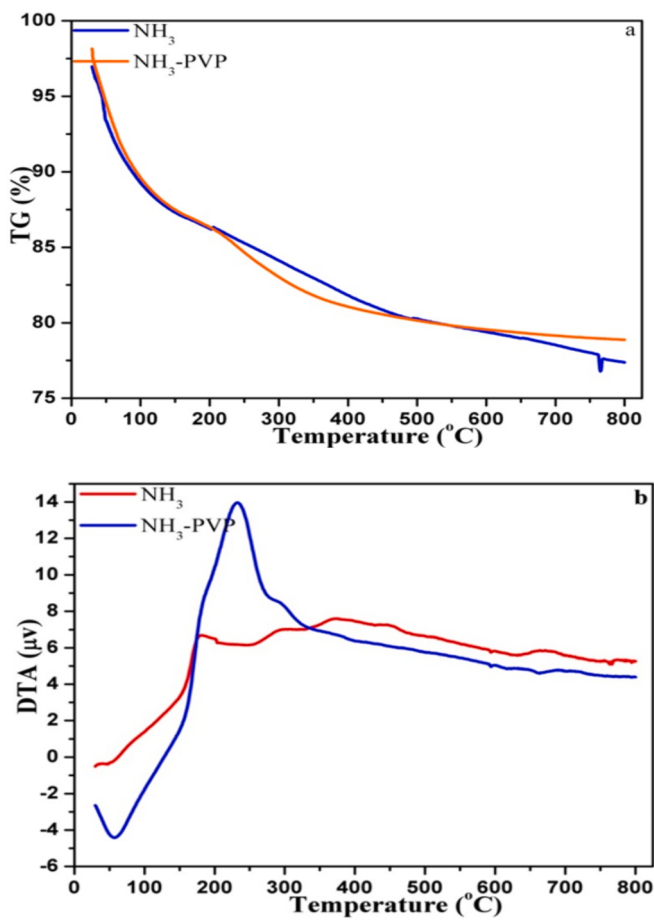


Fig. 7. a, b TG-DTA analysis of CeO_2 nanoparticles.

surface nitrate groups and subsequent production of nitric acid were suggested by second endothermic peak encountered from 120 to 220°C. Additionally, this explains the significant exothermic peak seen at 230 °C as shown in Fig. 7 (b). There was a significant weight loss occurred at third exothermic peak from 230 to 500°C. This exothermic peak points to the possible development of oxynitrate and dioxo nitrate complexes. For the compounds made of lanthanide, the creation of these complexes during heat degradation has been documented [42]. The complete formation of final product CeO_2 obtained at last endothermic peak only after 750 °C owing to the decomposition of dioxo nitrate. PVP strongly enhance the formation of oxynitrate and dioxo nitrate complexes due to appearance of exothermic peak at 230–500°C.

3.6. Compositional analysis

Fig. 8 (a-d) depicts the XPS spectrum of disk and slab shaped cerium oxide nanoparticles. The survey spectrum (Fig. 8a) revealed that the occurrence of Ce, O and C in the films. The samples surface only contains a little bit amount of Carbon that could be absorbed from the air. It indicates the high chemical purity of ceria nanoparticles. The Ce 3d core level spectra demonstrated that the mixed valance states of both Ce^{3+} and Ce^{4+} , due to its highly non-stoichiometric character. Five $3\text{d}_{3/2}$ - $3\text{d}_{5/2}$ spin-orbit-split doublets make up this system. The dominating peaks of $3\text{d}_{3/2}$ and $3\text{d}_{5/2}$ located at the binding energies 916.6 and 898.2 eV come from $\text{Ce } 3\text{d}^9 \text{O } 2\text{p}^6 \text{Ce } 4\text{f}^0$ final states of Ce^{4+} . The additional states of Ce^{4+} located at the binding energies 884.5, 901.3 and 908.1 eV result from a combination of $\text{Ce } 3\text{d}^9 \text{O } 2\text{p}^5 \text{Ce } 4\text{f}^1$ and $\text{Ce } 3\text{d}^9 \text{O } 2\text{p}^4 \text{Ce } 4\text{f}^2$ final states. A combination of $\text{Ce } 3\text{d}^9 \text{O } 2\text{p}^5 \text{Ce } 4\text{f}^2$ and $\text{Ce } 3\text{d}^9 \text{O } 2\text{p}^6 \text{Ce } 4\text{f}^1$ final states results in the contribution of Ce^{3+} states, which are positioned at 881.7 and 892.1 eV. Two additional weak 'shake-up' satellite peaks are

located at 893.9 and 913.7 eV due to the existence of + 3 and + 4 oxidation states. It also shows the fingerprint of CeO_2 phase with strong and sharp shoulder peak observed at 925.3 eV as shown in Fig. 8b. The overwhelming presence of CeO_2 and the slight presence of Ce_2O_3 were found in the Ce 3d core-electron levels. This suggests that Ce^{4+} ions are primarily found on the surface of CeO_2 NPs, which may have contributed further to the blue shift of CeO_2 NPs. This may be because the oxidation state changed from + 3 to + 4 which increased the charge transfer gap between $\text{O } 2\text{p}$ and $\text{Ce } 4\text{f}$ bands, which is consistent with PL results [43]. O 1s spectrum (Fig. 8c) consists of two broad peaks located at the binding energies 536.2 and 539.1 eV are assigned to the absorbed oxygen and hydroxyl groups on the surface of Ce respectively. C 1s spectrum confirms the presence of C in the samples as shown in (Fig. 8d). It has three peaks, which are categorized as follows: the higher intensity peak superposed around 291.3 eV due to the presence of carbonate species in the surface and also the peaks of lower intensity observed at 285.7 and 294.8 eV ascribed to the C—H and —CO₃ groups respectively. According to the calculations these ceria nanoparticles include 4.7 % of C, 12.07 % of O, 30.64 % of Ce^{3+} and 52.54 % of Ce^{4+} . Addition of PVP strongly promote the growth of Ce 3d peaks whereas faintly enhance the growth of C 1s peaks according to FT-IR results and shift the peaks towards higher binding energies as shown in Fig. 8 (a-d).

3.7. Photovoltaic characteristics

3.7.1. Fabrication details

Substrates made of Indium tin oxide (ITO) are bought from Delta Technologies, Ltd. (USA). Equivalent amounts of HCl and de-ionized water are combined with 1 ml of nitric acid to etch the substrate. The etched substrates were cleaned for 10 min each using deionized water and ethanol in an ultrasonic bath. In hetero-junction n- CeO_2 /p-CuInS₂, both CeO_2 and CuInS₂ were prepared by precipitation method and deposited on ITO substrates by JNSP technique. In this configuration CuInS₂ (CIS) nanoparticles are prepared by dissolving equal amount of copper nitrate ($\text{Cu } (\text{NO}_3)_2$) and indium chloride (InCl_3) in (50 ml) of deionized water and stirred for 1 hr. Then (25 ml) of ammonia solution is added to the above greenish blue solution, the colour of the solution changes to a deep blue. 0.15 M solution of thiourea ($\text{CS } (\text{NH}_2)_2$) is gradually added to the deep blue colored solution and continuously stirred for 3 hrs to get black colored precipitate [44]. The black precipitate is washed and dried at 373 K for 30 min. The obtained precipitate is dissolved in mixture of ethanol and water then deposited on ITO substrates at 200 °C by JNSP technique. The same procedure is followed for the deposition of CeO_2 . Vacuum evaporation technique is used to deposit ohmic contacts (Aluminium) on this window layer, with a uniform thickness 100 nm. For the other devices as well, the same process is used.

3.7.2. I-V characteristics

Photovoltaic output characteristics of spray-coated hetero-junction solar cells are depicted in Fig. 9(a-c). The calculations of power conversion efficiency (η) and fill factor (FF) for the hetero-junction solar cell are based on this plot. Since the dark features are rectifying in nature, it follows that under illumination, the device would show photovoltaic characteristics. In fact, devices operated as solar cells without a hole-transporting layer when illuminated by white light. In the figures, the corresponding device's open-circuit voltage (V_{OC}), short-circuit current density (J_{SC}), fill-factor (FF), and power conversion productivity (η) have been listed. However, the results showed that the samples prepared from NH_3 precipitant exhibited a high conversion efficiency 0.23 % and short circuit current density 0.361 mA/cm². The tendency of films to separate from the substrate and the development of pin holes in the film could be the cause of low value of short circuit current density. The cell's shunt resistance is determined to be 39.6 k Ω , while its series resistance is 2.49 k Ω based on its dark forward characteristics. The creation of high-quality films and the proper substrate temperature may be to blame for

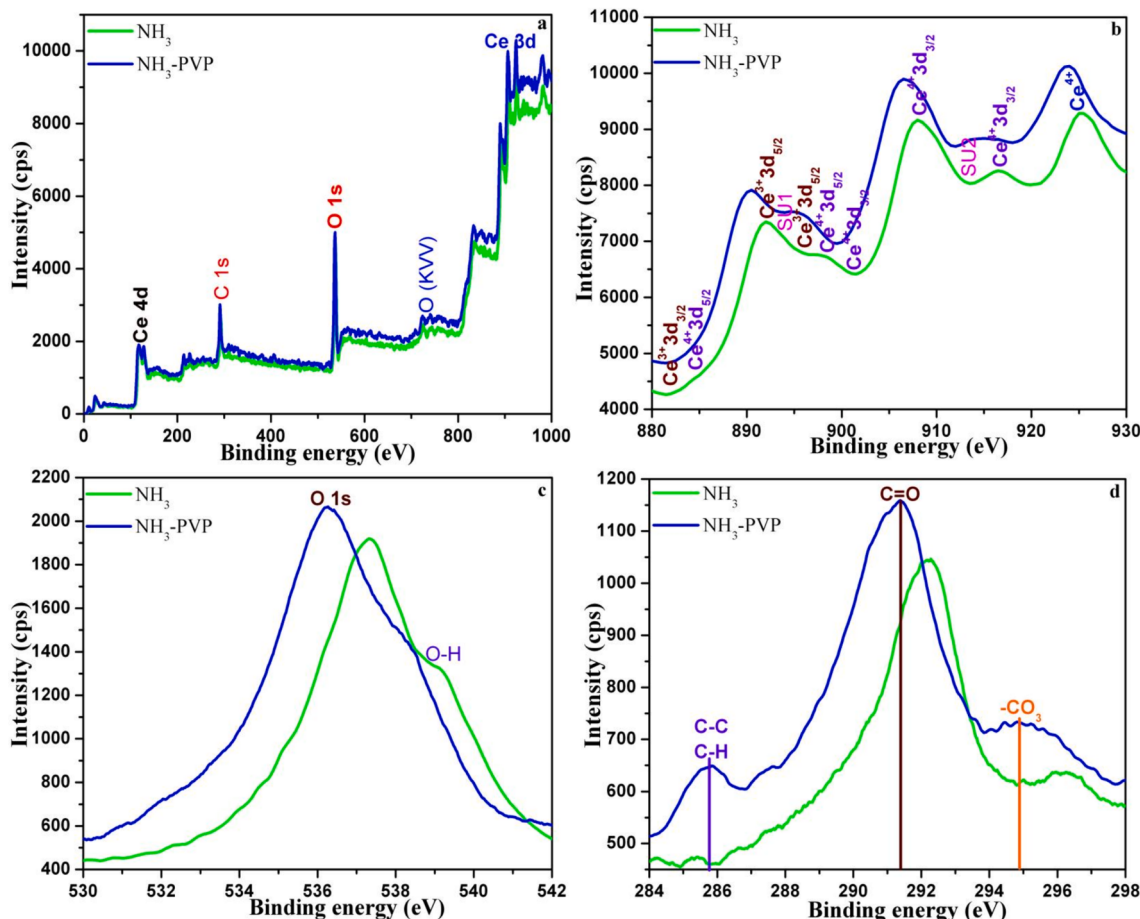


Fig. 8. A-d XPS spectra of CeO₂ nanoparticles.

the lower value of R_s for the film placed on ITO coated glass. The series resistance R_s and the shunt resistance R_{sh} have an impact on the values of η and FF [45]. The decrease in R_{sh} with thickness is similar to a decrease in η and is primarily connected to fill factor. These observed declines could be explained by an increase in leakage current caused by CIS sheet surface deuteration as well as an inter-diffusion of metals at the interface between ITO, CIS/CeO₂ and Al surface, which might encourage an increase in defects produced at this interface [46]. The minimum photovoltaic conversion efficiency was observed as 0.09 % for the samples made from KOH precipitant due to high sheet resistance, inferior crystal property and poor interfacial contact between metal, semiconductor and hetero-junction. G. Alan Sibu *et al.*, reported the good interfacial layer combination between metal and semiconductor contact and it gives high dielectric material is good for interfacial layer [47]. The morphological shape of the particles derived from various precipitants plays an essential role to authenticate the photovoltaic parameters and also promote the photovoltaic conversion efficiency [48,49]. Despite, this poor performance, it is still possible to increase it by fine-tuning the cell's processing and making the right connections with hole-transport and hole selective layers. This work paves the way for photon management properties employing thin films based on rare earth elements for application in photovoltaic devices.

4. Conclusion

CeO₂ nano-disk and nano-slap shaped particles are successfully synthesized used as cathode material by JNSP technique for solar cell applications. Various characterization techniques are employed to understand structural, optical, morphological, elemental and Photovoltaic properties of the synthesized particles. The XRD pattern reveals a single-

phase poly-crystalline face centered cubic CeO₂ crystallites. XPS and PL spectra provide the clear shows the presence of tetravalent Ce⁴⁺. The addition of PVP (polyvinylpyrrolidone) is strongly influence the growth of Ce 3d peaks, slightly enhance the growth of C 1s peaks and shift the peaks towards higher binding energies. SEM observations highlight the aggregates of spheroidal shaped particles, while TEM images exhibited agglomerated slap-like particles with curved edges and an average size of approximately 5 nm. Due to good interfacial contact between metals and hetero-junction layers, the device CIS/CeO₂ hetero-junction layers of the samples made from NH₃ exhibit the highest conversion efficiency of 0.23 %, the lowest series and shunt resistance and maximum short circuit current density in comparison to other prepared devices. Despite this low performance, it can be made much better by optimizing the cell processing and making adequate contacts with hole-transport and hole-selective layers. The precipitants and dispersant strongly modify the structural, optical, morphological, elemental as well as photovoltaic applications.

CRediT authorship contribution statement

P. Gayathri: Writing – original draft, Methodology. **T. Akila:** Writing – review & editing. **G. Alan Sibu:** Writing – review & editing. **Manickam Selvaraj:** Writing – review & editing. **Mohammed A. Assiri:** Writing – review & editing. **Priyadarshini matheswaran:** Writing – review & editing. **V. Balasubramani:** Writing – review & editing, Supervision.

Declaration of competing interest

The authors declare that they have no known competing financial

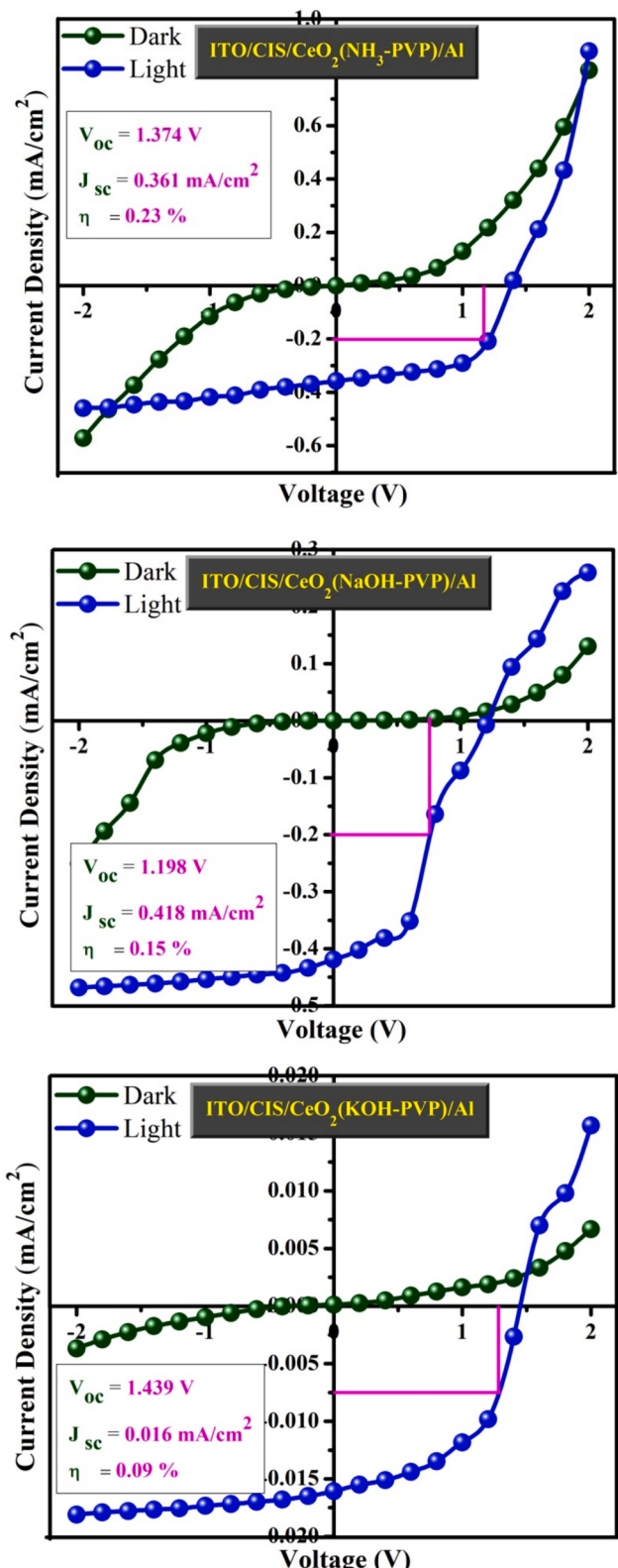


Fig. 9. A-c. I-V characteristics of spray-coated hetero-junction solar cells.

interests or personal relationships that could have appeared to influence the work reported in this paper.

Data availability

No data was used for the research described in the article.

Acknowledgements

The authors extend their appreciation to the Deanship of Scientific Research at King Khalid University for funding this work through the Large Project number 2/456/45 and the authors acknowledge the Research Center for Advance Materials (RCAMS) at King Khalid University, Saudi Arabia for their valuable technical support.

Data availability statement

The data that support the findings of this study are available from the corresponding author, upon reasonable request.

References

- [1] K. Gaurav Upadhyay, J.K. Rajput, T.K. Pathak, V. Kumar, L.P. Purohit, Synthesis of ZnO: TiO₂ nanocomposites for photocatalyst application in visible light, Vacuum 160 (2019) 154–163.
- [2] K.L. Chopra, P.D. Paulson, V. Dutta, Thin-film solar cells: an overview, Progress in Photovoltaics: Research and Applications 12 (2004) 69–92.
- [3] M. Nakamura, K. Tada, T. Kinoshita, T. Bessho, C. Nishiyama, I. Takenaka, Y. Kimoto, Y. Higashino, H. Sugimoto, H. Segawa, Perovskite/CIGS spectral splitting double junction solar cell with 28% power conversion efficiency, I Science 23 (2020) 101817.
- [4] D. Nurdan Sankir, E. Aydin, H. Unver, E. Uluer, M. Parlak, Preparation and characterization of cost-effective spray pyrolyzed absorber layer for thin film solar cells, Sol. Energy 95 (2013) 21–29.
- [5] V. Vishnu Kutwade, K.P. Gattu, M.E. Sonawane, D.A. Tonpe, I.M.S. Mohammed, R. Sharma, Theoretical modeling and optimization: Cd-free CTS/Zn(O, S)/ZnO thin film solar cell, Mater. Today Commun. 29 (2021) 102972.
- [6] A. Alizadeh, Z. Sharifiatinia, Unveiling the influence of SmFeO₃-TiO₂ nanocomposites as high performance photoanodes of dye-sensitized solar cells, J. Mol. Liq. 348 (2022) 118070.
- [7] V. Balasubramani, G. Alan Sibu, S. Kadaikunnan, J.M. Khaled, Proliferation in the photo-response characteristics of MDC thin films for optoelectronic applications through NSP technique, Sens. Actuators, A 366 (2024) 115008.
- [8] T. Minami, T. Miyata, Y. Nishi, Relationship between the electrical properties of the n-oxide and p-Cu₂O layers and the photovoltaic properties of Cu₂O-based heterojunction solar cells, Sol. Energy Mater. Sol. Cells 147 (2016) 85–93.
- [9] E. Kobayashi, Y. Watabe, T. Yamamoto, Y. Yamada, Cerium oxide and hydrogen co-doped indium oxide films for high-efficiency silicon heterojunction solar cells, Sol. Energy Mater. Sol. Cells 149 (2016) 75–80.
- [10] C. Wadia, A.P. Alivisatos, D.M. Kammen, Materials availability expands the opportunity for large-scale photovoltaics deployment, Environ. Sci. Tech. 43 (2009) 2072–2077.
- [11] N.K. Renuka, A.K. Praveen, C.U. Aniz, Ceria rhombic microplates: Synthesis, characterization and catalytic activity, Microporous and Mesoporous Materials 169 (2013) 35–41.
- [12] Q. Fu, H. Saltsburg, M. Flytzani-Stephanopoulos, Active non-metallic Au and Pt species on ceria-based water-gas shift catalysts, Science 301 (2003) 935–938.
- [13] P. Jasinski, T. Suzuki, H.U. Anderson, Nanocrystalline undoped ceria oxygen sensor, Sens. Actuators B 95 (2003) 73–77.
- [14] S. Thakur, P. Pradip, Rapid synthesis of cerium oxide nanoparticles with superior humidity-sensing performance, Sens. Actuators B 194 (2014) 260–268.
- [15] R. Li, S. Yabe, M. Yamashita, S. Momose, S. Yoshida, S. Yin, T. Sato, Synthesis and UV-shielding properties of ZnO-and CaO-doped CeO₂ via soft solution chemical process, Solid State Ion. 151 (2002) 235–241.
- [16] B.C.H. Steele, A. Heinzel, Materials for fuel-cell technologies, Nature 414 (2001) 345–352.
- [17] A. Mondal, A. Zachariah, P. Nayak, B.B. Nayak, Synthesis and room temperature photoluminescence of mesoporous zirconia with a tetragonal nanocrystalline framework, J. Am. Ceram. Soc. 93 (2010) 387–392.
- [18] W. Yuan, H.Z. Zhang, Q. Liu, G.R. Li, X.P. Gao, Surface modification of Li(Li_{0.17}Ni_{0.2}C_{0.05}Mn_{0.58}O₂)₂ with CeO₂ as cathode material for Li-ion batteries, Electrochimica Acta 135 (2014) 199–207.
- [19] J.L. Mac Manus-Driscoll, S.R. Foltyn, Q.X. Jia, H. Wang, A. Serquis, L. Civale, B. Maiorov, M.E. Hawley, M.P. Maley, D.E. Peterson, Strongly enhanced current densities in superconducting coated conductors of YBa₂Cu₃O_{7-x}+ BaZrO₃, Nat. Mater. 3 (2004) 439–443.
- [20] M. Akhlouch, A. Calleja, X. Granados, S. Ricart, V. Boffa, F. Ricci, T. Puig, X. Obradors, Hybrid sol-gel layers containing CeO₂ nanoparticles as UV-protection of plastic lenses for concentrated photovoltaics, Sol. Energy Mater. Sol. Cells 120 (2014) 175–182.
- [21] X. Feng, D.C. Sayle, Z.L. Wang, M.S. Paras, B. Santora, A.C. Sutorik, T.X.T. Sayle, et al., Converting ceria polyhedral nanoparticles into single-crystal nanospheres, Science 312 (2006) 1504–1508.
- [22] D. Chen, Y. Wang, M. Hong, Lanthanide nanomaterials with photon management characteristics for photovoltaic application, Nano Energy 1 (2012) 73–90.
- [23] H. Lian, Z. Hou, M. Shang, D. Geng, Y. Zhang, J. Lin, Rare earth ions doped phosphors for improving efficiencies of solar cells, Energy 57 (2013) 270–283.
- [24] P. Harish Senthil, J. Chandrasekaran, R. Marnadu, V. Balasubramani, Incorporation of Zn ions on high dielectric HfO₂ thin films by spray pyrolysis and

- fabrication of Al/Zn@ HfO₂/n-Si Schottky barrier diodes, *Sens. Actuators, A* 331 (2021) 112725.
- [25] Y.W. Zhang, R. Si, C.-S. Liao, C.-H. Yan, C.-X. Xiao, Y. Kou, Facile alcothermal synthesis, size-dependent ultraviolet absorption, and enhanced CO conversion activity of ceria nanocrystals, *J. Phys. Chem. B* 107 (2003) 10159–10167.
- [26] B. Gowtham, V. Ponnuswamy, J. Chandrasekaran, V. Balasubramani, R. Suresh, G. Pradeesh, S. Ramanathan, Effect of surface modification of WO₃ nanostructures on the performance for p-Si/n-WO₃ structure diodes, *Inorg. Chem. Commun.* 130 (2021) 108695.
- [27] S. Phoka, P. Laokul, E. Swatsitang, V. Promarak, S. Seraphin, S. Maensiri, Synthesis, structural and optical properties of CeO₂ nanoparticles synthesized by a simple polyvinyl pyrrolidone (PVP) solution route, *Mater. Chem. Phys.* 115 (2009) 423–428.
- [28] R. Suresh, V. Ponnuswamy, R. Mariappan, Effect of annealing temperature on the microstructural, optical and electrical properties of CeO₂ nanoparticles by chemical precipitation method, *Appl. Surf. Sci.* 273 (2013) 457–464.
- [29] S.Y. Chen, C.-H. Tsai, M.-Z. Huang, D.-C. Yan, T.-W. Huang, A. Gloter, C.-L. Chen, H.-J. Lin, C.-T. Chen, C.-L. Dong, Concentration dependence of oxygen vacancy on the magnetism of CeO₂ nanoparticles, *J. Phys. Chem. C* 116 (2012) 8707–8713.
- [30] G.E. Putri, Y. Rilda, S. Syukri, A. Labanni, S. Arief, Highly antimicrobial activity of cerium oxide nanoparticle synthesized using *Moringa oleifera* leaf extract by a rapid green precipitation method, *J. Mater. Res. Technol.* 15 (2021) 2355–2364.
- [31] A. Turkovic, Z. Crnjak Orel, Dye-sensitized solar cell with CeO₂ sub 2 and mixed CeO₂ sub 2/SnO₂ (sub 2 photoanodes, *Sol. Energy Mater. Sol. Cells* 45 (1997).
- [32] M. Lira-Cantu, C. Krebs Frederik, Hybrid solar cells based on MEH-PPV and thin film semiconductor oxides (TiO₂, Nb₂O₅, ZnO, CeO₂ and CeO₂–TiO₂): Performance improvement during long-time irradiation. <https://doi.org/10.1016/j.solmat.200.6.007>.
- [33] Y.M. Kang, S.H. Kwon, P.K. Song, Study on mechanical and electro-optical properties of ITO/CeO₂ films deposited on PI substrate for flexible organic solar cells, *Curr. Appl. Phys.* 10 (2010) S491–S494.
- [34] N.K. Renuka, Structural characteristics of quantum-size ceria nano particles synthesized via simple ammonia precipitation, *J. Alloy. Compd.* 513 (2012) 230–235.
- [35] C. Chai, S. Yang, Z. Liu, M. Liao, N. Chen, Violet/blue photoluminescence from CeO₂ thin film, *Chin. Sci. Bull.* 48 (2003) 1198–1200.
- [36] C. Sun, H. Li, H. Zhang, Z. Wang, L. Chen, Controlled synthesis of CeO₂ nanorods by a solvothermal method, *Nanotechnology* 16 (2005) 1454.
- [37] K.M. Khalil, S. Leena A. Elkabee, B. Murphy, Preparation and characterization of thermally stable porous ceria aggregates formed via a sol-gel process of ultrasonically dispersed cerium (IV) isopropoxide, *Microporous and Mesoporous Materials* 78 (2005) 83–89.
- [38] Y. Zhang, Y. Lin, C. Jing, Y.H. Qin, Formation and thermal decomposition of cerium-organic precursor for nanocrystalline cerium oxide powder synthesis, *J. Dispers. Sci. Technol.* 28 (2007) 1053–1058.
- [39] M. Daniel Lyons, K.M. Ryan, M.A. Morris, Preparation of ordered mesoporous ceria with enhanced thermal stability, *J. Mater. Chem.* 12 (2002) 1207–1212.
- [40] R. Srinivasan, A. Chandra Bose, Structural properties of Sm³⁺ doped cerium oxide nanorods synthesized by hydrolysis assisted co-precipitation method, *Mater. Lett.* 64 (2010) 1954–1956.
- [41] H.W. He, X.-Q. Wu, W. Ren, P. Shi, X. Yao, Z.-T. Song, Synthesis of crystalline cerium dioxide hydrosol by a sol-gel method, *Ceram. Int.* 38 (2012) S501–S504.
- [42] A.I.Y. Tok, F.Y.C. Boey, Z. Dong, X.L. Sun, Hydrothermal synthesis of CeO₂ nanoparticles, *J. Mater. Process. Technol.* 190 (2007) 217–222.
- [43] G. Wang, M. Qiuying, T. Chen, Y. Wang, Synthesis, characterization and photoluminescence of CeO₂ nanoparticles by a facile method at room temperature, *J. Alloy. Compd.* 493 (2010) 202–207.
- [44] H. Pervaiz, Z.S. Khan, N. Shahzad, G. Ali, N. Iqbal, S. Javed, Fabrication of cellulose paper-based counter electrodes for flexible dye-sensitized solar cells, *PCCP* 25 (2023) 428–438.
- [45] V. Damodara Das, Damodara. Laxmikant, A study of band-bending and barrier height variation in thin film n-CdSe_{0.5}Te_{0.5} photoanode/polysulphide junctions, *Solid State Commun.* 99 (1996) 723–728, [https://doi.org/10.1016/0038-1098\(96\)00195-0](https://doi.org/10.1016/0038-1098(96)00195-0).
- [46] T. Minami, Y. Nishi, T. Miyata, J.-I. Nomoto, High-efficiency oxide solar cells with ZnO/Cu₂O heterojunction fabricated on thermally oxidized Cu₂O sheets, *Appl. Phys. Express* 4 (2011) 062301.
- [47] G. Alan Sibu, P. Gayathri, T. Akila, R. Marnadu, V. Balasubramani, Manifestation on the choice of a suitable combination of MIS for proficient Schottky diodes for optoelectronics applications: a comprehensive review, *Nano Energy* (2024) 109534.
- [48] T. Akila, P. Gayathri, G. Alan Sibu, V. Balasubramani, Hamad Al-Lohedan, M. Al-Dhayan Dhaifallah, Augmented photovoltaic performance of Cu/Ce-(Sn: Cd)/n-Si Schottky barrier diode utilizing dual-doped Ce-(Sn: Cd) thin films, *Opt. Mater.* 149 (2024) 115133.
- [49] T. Sasikala, K. Shanmugasundaram, P. Thirunavukkarasu, P. Vivek, Impact of phase transformation on MoS₂ thin films on high temperature and its concomitant role in In-MoS₂/P-Si structured PN junction diodes, *Opt. Mater.* 131 (2022) 112584.